(Received 29 July 2025, Accepted 30 September 2025, Scheduled 15 November 2025)

Design and Optimization of a Dual-Band F-Shaped Monopole Antenna for 2.45/5.8 GHz ISM Medical Applications Using ANN and PSO

Rania Ibtissam Ben Melouka[1], Yamina Tighilt[2], Chemseddine Zebiri[1,*], Issa Elfergani[3,4], Rami Zegadi[1], Mohamed Lamine Bouknia[1], Abdelhak Ferhat Hamida[2], Merih Palandoken[5], Fatih Özkan Alkurt[6], Muharrem Karaaslan[6], Nail Alaoui[7], and Jonathan Rodriguez[3]

[1]*Laboratoire d'Electronique de Puissance et Commande Industrielle (LEPCI) Department of Electronics, University of Ferhat Abbas, Setif-1, Setif 19000, Algeria*
[2]*Laboratoire d'Instrumentation Scientifique (LIS), Department of Electronics, Faculty of Engineering University of Ferhat Abbas, Setif-1, Setif 19000, Algeria*
[3]*Instituto de Telecomunicações, Campus Universitário de Santiago, 3810-193, Aveiro, Portugal*
[4]*Faculty of Engineering and Informatics, University of Bradford, Bradford, UK*
[5]*Faculty of Engineering and Natural Sciences, Department of Electrical and Electronics Engineering Izmir Katip Çelebi University, Izmir 35620, Türkiye*
[6]*Faculty of Engineering and Architecture, Department of Electrical and Electronics Engineering Iskenderun Technical University, Hatay 31200, Türkiye*
[7]*Laboratoire de Modélisation, Simulation et Optimisation des Systèmes Complexes Réels University of Djelfa, Djelfa 17000, Algeria*

ABSTRACT: The article presents the geometry and optimization of a small-sized dual-band F-shaped monopole antenna for medical applications in the 2.45/5.8 GHz ISM bands. The antenna is printed on a partial ground FR4 substrate, and its geometrical parameters are optimized using Artificial Neural Networks (ANNs) and Particle Swarm Optimization (PSO). Two ANN architectures, Feedforward Backpropagation Neural Network (FFBPN) and Generalized Regression Neural Network (GRNN), are trained on a dataset of 121 samples generated using varying patch sizes. The FFBPN model is better with a mean squared error of 3.9506×10^{-5} at epoch 21. The optimized antenna has resonances at 2.448 GHz and 5.8 GHz with $S_{11} < -10$dB, bandwidths of 610 MHz (2.21-–2.82 GHz) and 400 MHz (5.61–-6.01 GHz), and peak gains of 2.262 dBi and 3.9 dBi, respectively. Measurements on a prototype are in agreement with simulations to confirm the appropriateness of the design for wireless medical devices, such as wearable sensors and telemedicine systems.

1. INTRODUCTION

Antennas are essential for wireless communication systems because they interact with electromagnetic waves as front-end devices in free space. Current communication systems use antennas for many applications, including portable wireless devices [1–3], radar systems [4, 5], and other medical applications [6–10]. Monopole antennas have specific prominence in biomedical engineering not only because of their user-friendly design but also their ease to manufacture and reliability [11, 12]. A monopole antenna is capable of wireless communication between medical devices which enables remote monitoring of vital physiological data such as blood pressure and ECG readings [3, 13–19]. The increasing demand for small, flat, dual-band antennas operating within the 2.45/5.8 GHz Industrial, Scientific, and Medical (ISM) bands originates from applications in wireless health monitoring, implantable sensors, and wearable healthcare devices [3, 6–8, 13, 17, 19]. Antennas that operate in the 2.45/5.8 GHz bands will facilitate the real-time transmission of physiological data as they support telemedicine applications connecting patients who are well beyond the reach of a medical provider [20, 21].

Dual-band antennas have numerous applications in wireless body area networks (WBANs) [7, 22–27], RFID systems [28], WLAN [29], and biomedical devices [30–44]. Although the designs of dual-band antennas are many, some basic engineering criteria include: low dimensions, acceptable radiation characteristics, simple configurations, low profiles, manageable gains, and high efficiencies [45]. Some design solutions have been presented for ISM band applications. A chip antenna designed for the 2.4 GHz band indicated a gain of 3.5 dBi with 126 MHz bandwidth [46]. A wire antenna on an FR-4 substrate indicated a gain of 2 dBi and bandwidth of 200 MHz. An inverted-F antenna exhibited 2.5 dBi of gain [47], and another example possessed 1.5 dBi of gain [48] which revealed quasi-omnidirectional radiation patterns [49]. Compact monopole designs with proper bandwidth yielded 1.354 dBi of gain with 330 MHz bandwidth [50], although a microstrip antenna designed using shorting pins demonstrates 0 dBi gain [51]. The microstrip line feeding showed effectiveness in impedance

* Corresponding author: Chemseddine Zebiri (czebiri@univ-setif.dz).

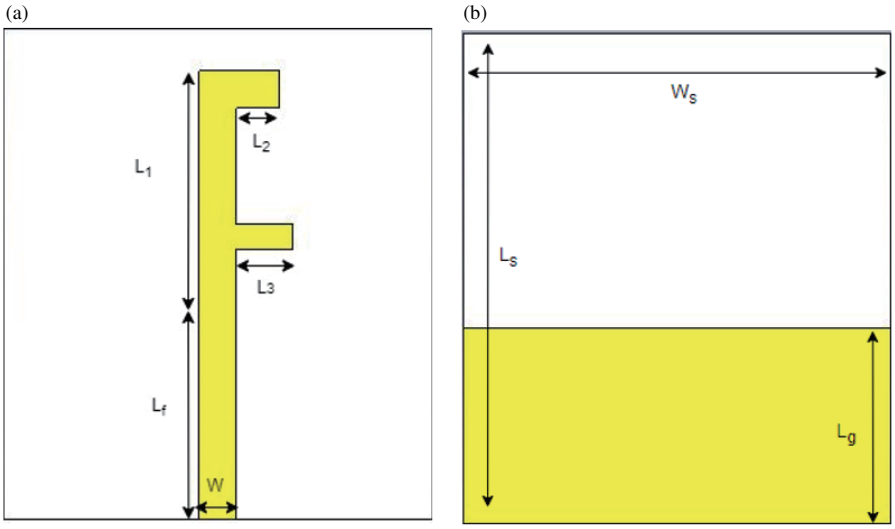

FIGURE 1. The proposed antenna front and back views.

matching and gain objective [25]. The dielectric resonator antenna from literature evidenced a gain of 5.5 dBi [52].

Recent progress includes the development of small-form printed antennas for medical applications [53–55], fractal antenna designs optimized by PSO [56, 57], and using spiral structures with coverage in MICS and ISM bands [58], Dual-band antennas for WiFi applications were inspired from fractal Hilbert curves [59]. Artificial Neural Networks (ANNs) can assist in the optimization process of an antenna design, with some specific layer architectures being feed forward back propagation network (FFBPN) [60] and General Regression Neural Networks (GRNNs) [61]. Despite previous work on dual-band ISM antennas and optimization methods such as PSO [30–32], as well as review of ANN techniques in medical applications, the use of ANN with PSO to aid in medical antennas design is less documented [57, 58]. This research will establish this by providing optimization design methods based on ANNs and PSO for a dual-band monopole antenna.

Our main contributions include:

- An optimization framework employing both ANNs and PSO for antenna parameter prediction
- A compact dual-band design operating at 2.448 GHz (610 MHz bandwidth) and 5.8 GHz (400 MHz bandwidth)
- Peak gains of 2.262 dBi and 3.9 dBi at respective frequencies
- Comprehensive validation through simulation and measurement

The paper is organized as follows. Section 2 describes the antenna design. Section 3 presents numerical specifications. Section 4 details the numerical analysis and ANN modeling. Sections 5–6 explain curve fitting and PSO optimization. Section 7 presents performance evaluation, and Section 8 concludes the work.

2. ANTENNA DESIGN AND CONFIGURATION

Figure 1 shows the proposed dual-band planar antenna design. The F-shaped radiating element is printed on an FR4 substrate ($\epsilon_r = 4.3$, thickness = 1.6 mm, $\tan\delta = 0.019$) with a truncated ground plane. A 50 Ω microstrip feed line (width = 3 mm) designed using transmission line theory [25] is connected to an SMA port for excitation.

2.1. Antenna Design

A planar monopole antenna was designed for dual-band operation at 2.45 GHz and 5.8 GHz, targeting medical applications in the ISM bands. The antenna dimensions were determined using transmission line theory [25, 62], with key parameters calculated through the following analytical approach.

2.2. Dimensional Calculations

The effective dielectric constant (ε_{reff}) and length extension were computed using:

$$\varepsilon_{reff} = \frac{\varepsilon_r + 1}{2} + \frac{\varepsilon_r - 1}{2}\left(1 + 12\frac{h}{w}\right)^{-0.5} \quad (1)$$

where:

- ε_r = dielectric constant of substrate
- w = width of radiating patch
- h = substrate height

The effective resonant length (L_{eff}) was derived from surface current distributions, corresponding to quarter-wavelength resonance:

$$L_{eff} = \frac{v_0}{2f_r\sqrt{\varepsilon_{reff}}} \quad (2)$$

where v_0 is the speed of light in free space, and f_r is the resonant frequency.

TABLE 1. Geometrical parameters of the proposed antenna.

Parameters	Value (mm)	Parameters	Value (mm)
L_1	19	L_f	17.5
L_2	3.5	$W_s = W_g$	35
L_3	4.6	L_s	40
L_4	3	L_g	16
L_5	2	W	3

2.3. Antenna Parameters

The complete geometrical parameters of the proposed design are summarized in Table 1. These dimensions were optimized to achieve dual-band operation while maintaining compact form factor suitable for medical applications.

The design achieves resonance at both target frequencies through careful control of the patch geometry and ground plane configuration, as described in the following sections.

3. ANN MODEL

The Artificial Neural Network (ANN) serves as a powerful tool for establishing a relationship between the antenna's geometrical parameters and its resonant frequencies. Utilizing the feedforward backpropagation model, the ANN is structured into three primary layers: input layer, hidden layer, and output layer. The input layer is composed of neurons that correspond to the input vector dimensions $X = \{x_1, x_2, x_3, x_4, \ldots, x_n\}$, each representing a distinct input parameter. The outputs of these input neurons are fed into the hidden layer, which processes the data and passes the results to the output layer. The crucial task of determining the optimal weights for the connections between neurons, known as training the network, ensures that the ANN accurately models the relationship between inputs and outputs. Fig. 2 illustrates the developed feedforward backpropagation network (FFBPN) model applied to the proposed compact dual-high frequency antenna design. Table 2 illustrates the parametric configuration of the ANN. In the proposed FFBPN model, the two inputs consist of the geometrical parameters of the patch, while the outputs correspond to the resonant frequencies. The dataset is generated using CST software, comprising 121 randomly generated samples along with their corresponding resonant frequencies, f_{r1} and f_{r2}. Of these 121 samples, 85 are utilized for training the network, while the remaining 18 are reserved for testing and validation purposes. The model's performance is evaluated based on the error value obtained during this process. The error is calculated using the following expression:

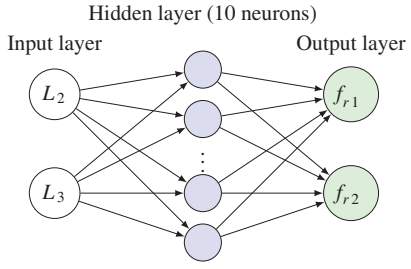

FIGURE 2. ANN-based analysis model (Feedforward Backpropagation Network).

TABLE 2. ANN-based analysis model for the proposed antenna.

ANN parameters	Values
Number of inputs (L_2, L_3)	2
Number of outputs (f_{r1}, f_{r2})	2
Number of hidden neurons	10
Number of epochs	1000
Training algorithm	Levenberg-Marquardt

$$\text{Absolute Error} = |\text{Simulated Outcome} - \text{ANN Model Outcome}| \quad (3)$$

4. CURVE FITTING APPROACH

The primary aim of this technique is to depict empirical data using a model, such as a function or mathematical equation and assess the parameters linked to that model. In simple terms, it offers the most accurate depiction of experimental data by employing a mathematical model. It calculates the coefficient values that result in a function closely approximating the given data set. This study employs a curve-fitting method to establish a straightforward mathematical correlation between the parameter values L_2 and L_3 and related operating frequencies (f_{r1} and f_{r2}). A data collection including 121 samples is generated randomly by selecting various parameters. By employing this methodology, the subsequent pair of mathematical equations is produced.

The MATLAB software enables the creation of curves, surfaces, and mathematical functions through the process of curve fitting. This technique facilitates the establishment of a practical correlation between observed data and parameter values, resulting in the optimal alignment with the data set. The primary methodologies for curve fitting are least squares regression and interpolation. The current study utilises the curve-fitting technique to establish a correlation between parameter values and the corresponding resonant frequencies (f_{r1} and f_{r2}). The data set of 121 samples is obtained by systematically altering the parameter values L_2 and L_3 of the proposed antenna. The selected range of L_2 is 2.5 to 4.5 mm and L_3 is 3 to 5 mm. The resonant frequency corresponding to each sample is noted down.

Based on this data set, the equations for f_{r1} and f_{r2} are derived and presented in Eqs. (4) and (5).

$$fr_1 = -0.05375L_2 - 0.0007603L_3 + 2.638 \quad (4)$$

$$fr_2 = -0.09278L_2 - 0.345L_3 + 7.716 \quad (5)$$

5. PSO REALIZATION

PSO technique, first proposed by Dhaliwal and Pattnaik [56], is characterised by its efficient utilisation of the cooperative behaviour exhibited by particles. A set of particles with randomly assigned positions is defined in an N-dimensional design space. The positions of these particles are updated in each iteration

based on velocity updates [63]. Once the position and velocity of each particle in the population have been set, the velocity of each particle is updated [57]. In each iteration, every particle modifies its position based on its current position, current velocity, the distance to its personal best position (pbest), and the distance to the global best position (gbest) [63].

The selection of the fitness or cost function is meticulously made to guarantee optimal performance of PSO algorithm. The design space and cost function are unique to the optimisation problem. The PSO algorithm employs Eqs. (6) and (7) to update the velocity and position of each particle [57]:

$$v_i(t+1) = wv_i(t) + c_1 r_1 \left[pbest(t) - x_i(t)\right] + c_2 r_2 \left[gbest(t) - x_i(t)\right]. \quad (6)$$

$$x_i(t+1) = x_i(t) + v_i(t+1) \quad (7)$$

where v_i represents the particle's velocity; x_i represents the particle's position; w is the inertial weight; c_1 and c_2 are acceleration constants, both having a value of 1.5.

The algorithm concludes when a satisfactory solution is achieved. An objective function is formulated to guarantee that the proposed antenna achieves resonance at frequencies specified by the user, as represented by Eq. (8). Fig. 3 displays the comprehensive flowchart of the PSO algorithm used to calculate parameters L_2 and L_3.

$$\text{cost function} = \sqrt{(2.45 - f_{r1})^2 + (5.8 - f_{r2})^2} \quad (8)$$

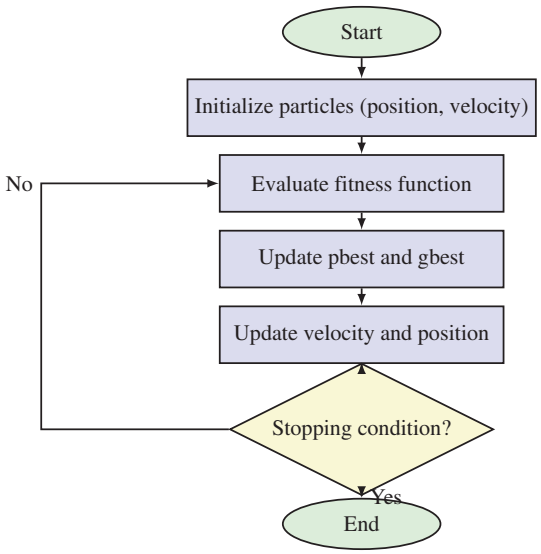

FIGURE 3. Flowchart of the PSO algorithm.

6. RESULTS AND DISCUSSIONS

The evaluation of the antenna's performance is conducted through a thorough approach that encompasses the development, modelling, and analysis of its radiating structure using CST. When the antenna is excited via a waveguide port, essential performance metrics such as directivity, voltage standing wave ratio (VSWR), gain, reflection coefficient, surface electric field, and far-field pattern are evaluated.

By integrating open add-space boundary conditions into the simulations, a comprehensive assessment of the antenna's performance and behaviour is attained. This method offers a precise representation of how the antenna interacts with the surrounding environment. This methodology provides valuable insights into the effectiveness, focussing capability and dispersion of electromagnetic fields of the antenna, allowing for optimisation based on specific design criteria.

6.1. Bandwidth and Scattering Parameters S_{11}

The objective of the design being discussed is to attain dual-band capabilities specifically for medical applications. It has been achieved by utilising an antenna design featuring a modified radiation patch. Fig. 4 compares the return loss characteristics of three different antennas: the rectangular monopole antenna (Fig. 4(a)), the antenna with an L inverse-shaped radiating patch (Fig. 4(b)), and the antenna with a modified F-shaped radiator (Fig. 4(c)).

In order to assess the effectiveness of the proposed antenna, a frequency range spanning from 1 to 9 GHz was chosen for analysis. The two frequency sub-bands of interest are 2.21–2.82 GHz and 5.61–6.01 GHz, with center frequencies of 2.448 GHz and 5.8 GHz, respectively.

In the first design, the antenna resonates at 2.645 GHz and 7.3 GHz, exhibiting S_{11} values of -24.4 dB and -11.99 dB, respectively, as illustrated in Fig. 5. The second design of the antenna resonates at 2.33 GHz and 5.58 GHz, exhibiting S_{11} values of -25.445 dB and -18.95 dB, respectively. The proposed antenna functions within the ISM frequency bands, specifically (2.4–2.5 GHz) and (5.61–6.01 GHz).

The S_{11} values of -27.97 dB and -14.63 dB are measured at the respective resonant frequencies. The bands utilise frequencies of 610 MHz (2.21–2.82 GHz) and 400 MHz (5.61–6.01 GHz). The specified bandwidth of 610 MHz is greater than the usual range of frequencies for the ISM band, which is from 2.4 to 2.4835 GHz. On the other hand, the 400 MHz bandwidth fits well within the higher frequencies of the ISM bands, which range from 5.725 to 5.875 GHz. These bands are designated for non-communication uses; however, they can be utilised for communication within certain regulations, such as Wi-Fi, Bluetooth, and selecting cordless phones. Fig. 6 shows the S_{11} plot containing simulated values.

6.2. Gain and Directivity

Gain and directivity are crucial factors for evaluating the performance of an antenna. Figs. 7(a) and 7(b) depict the three-dimensional gain patterns of the proposed antenna for frequencies of 2.45 GHz and 5.8 GHz, respectively. Figs. 8(a) and 8(b) display the three-dimensional directivity plots that correspond to the same frequencies. The maximum gain values are 3.9 dB at a frequency of 2.45 GHz and 5.2 dB at a frequency of 5.8 GHz. At these frequencies, the directivity peaks are 3.9 dB and 5.2 dB, respectively.

The antenna under consideration has an efficiency of roughly 87%, and at the resonant frequency of 5.8 GHz, the efficiency is approximately 74%.

Figure 9 illustrates the peak gain versus frequency. The antenna gain is calculated as 2.262 dB and 3.9 dB for the resonant

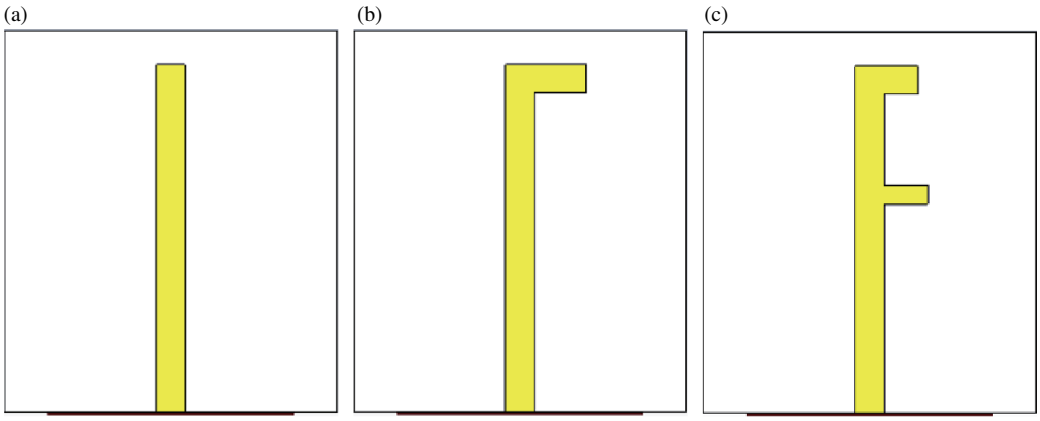

FIGURE 4. Antenna structure. (a) Base structure.. (b) L inverse-shaped. (c) F-shaped.

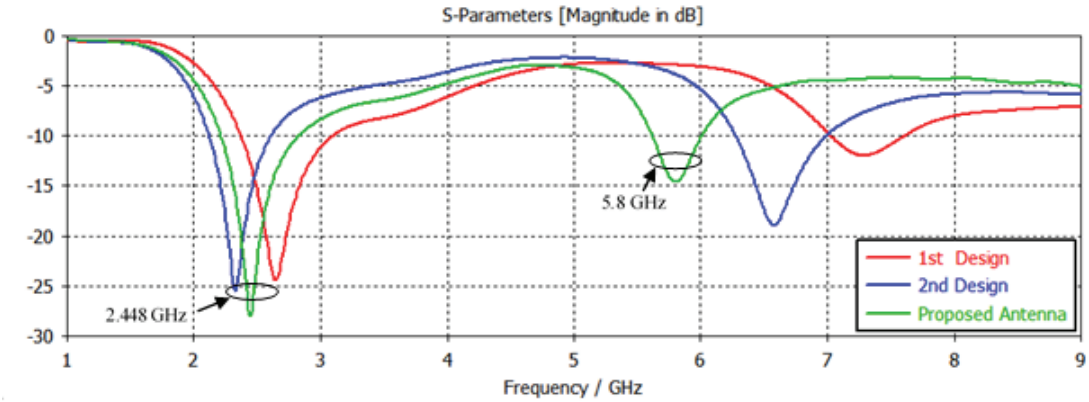

FIGURE 5. S_{11} parameter comparison across three antenna design iterations.

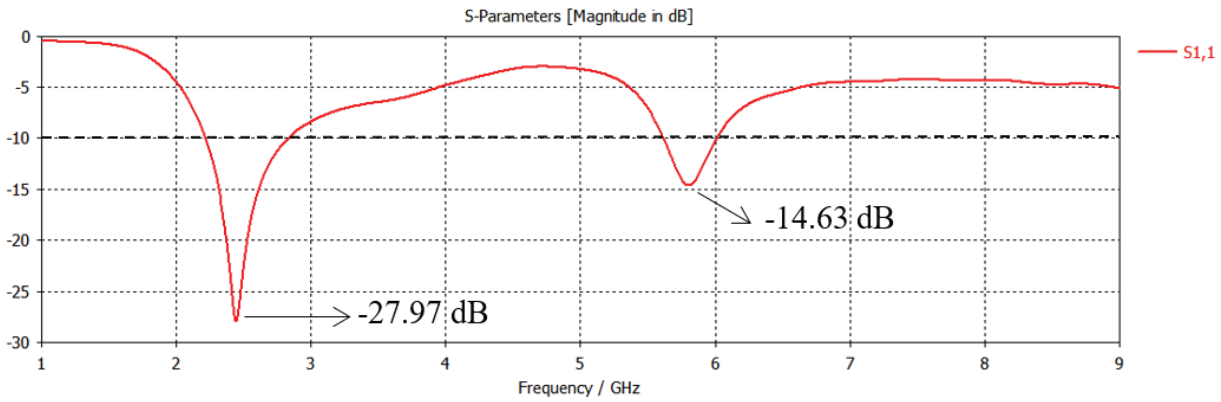

FIGURE 6. Simulated S_{11} characteristics of the proposed antenna.

frequencies of 2.45 GHz and 5.8 GHz, respectively. A 2.262 dB gain is generally moderate but may be adequate for communication over short distances, such as within a hospital room or between body-worn sensors and a receiver in close proximity. Reducing the gain can also be beneficial in minimising the possibility of interaction with other devices and ensuring safety. Medical gadgets are required to adhere to stringent safety standards and regulations. Using antennas with lower gain might decrease the specific absorption rate (SAR), thereby ensuring the safety of the device for human use. A 3.9 dB value at 5.8 GHz offers a slightly greater level of performance, which can be advantageous for applications that demand longer range or larger data rates.

6.3. Current Distribution

Surface current distribution refers to the spatial arrangement of current density across a patch, indicating current density variation at different frequencies of operation. Figs. 10 and 11

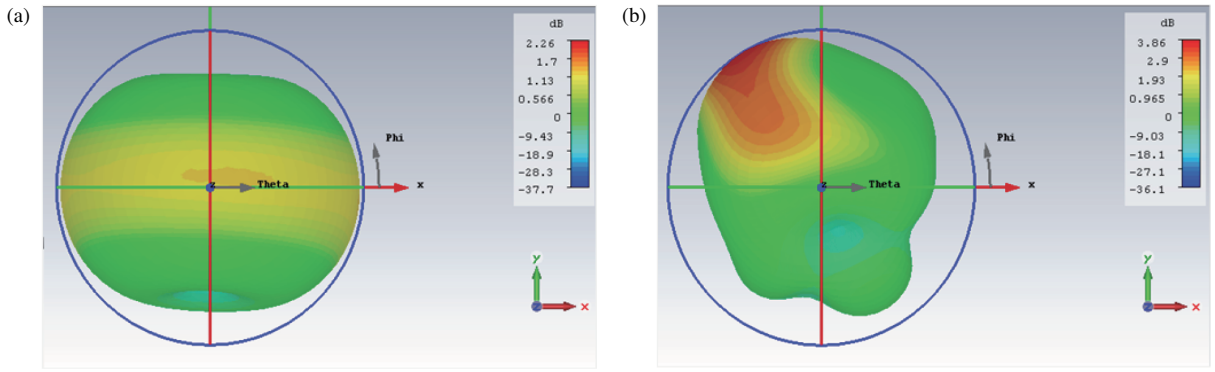

FIGURE 7. 3D gain plot of proposed antenna at (a) 2.45 GHz. (b) 5.8 GHz.

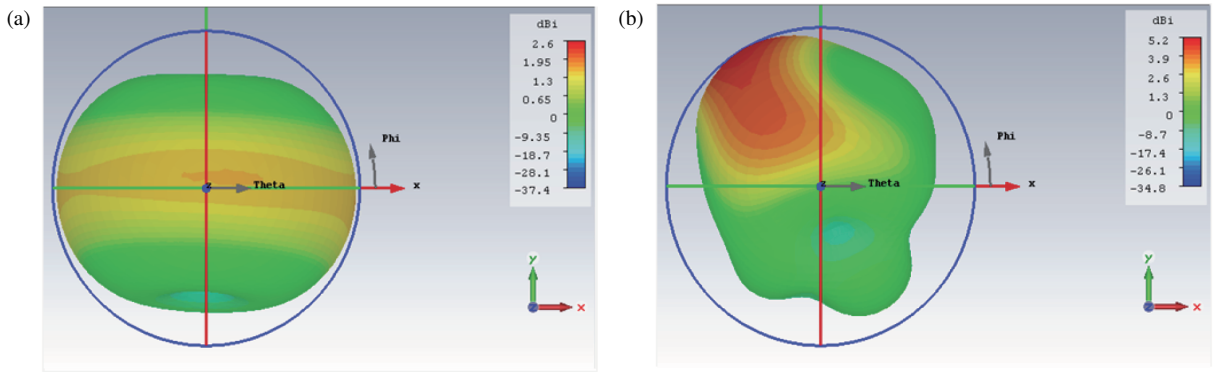

FIGURE 8. 3D directivity plot of proposed antenna at (a) 2.45 GHz. (b) 5.8 GHz.

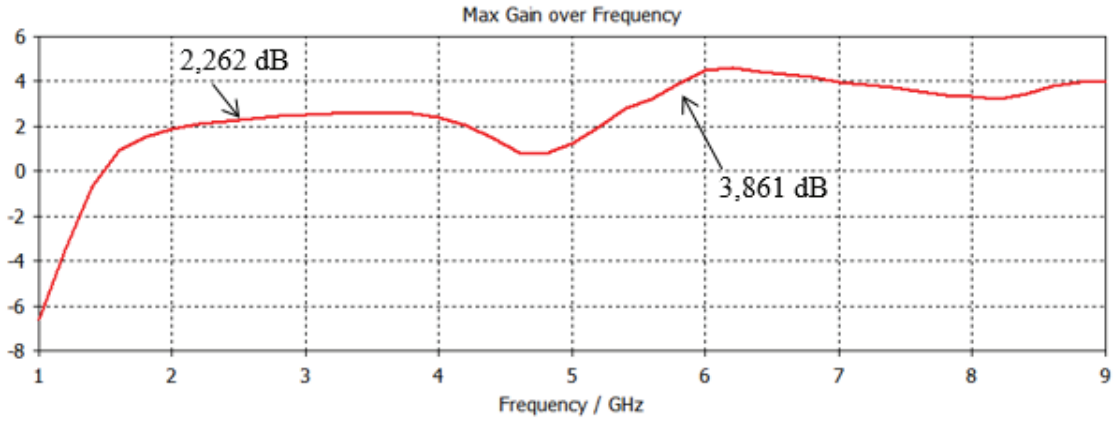

FIGURE 9. Peak gain of the proposed antenna.

display the surface current distribution plots at specific resonant frequencies for the proposed antenna. The analysis demonstrates that the highest current density is achieved at the feed, indicating a significant coupling effect. The monopole antenna exhibits the lowest current density at its upper section. The current distribution on the monopole antenna confirms its favourable radiation characteristics and showcases enhanced performance in relation to the reflection coefficient and impedance matching.

6.4. Radiation Pattern

The radiation pattern of the antenna is shown in Figs. 12 and 13. The antenna is linearly polarized; therefore, its E- and H-plane patterns are analyzed to gain insight into its radiation characteristics in the two orthogonal planes. Pattern analysis reveals that the proposed antenna exhibits figure-of-eight radiation characteristics in the E-plane (XZ) and produces a similar figure-of-eight pattern in the H-plane (YZ).

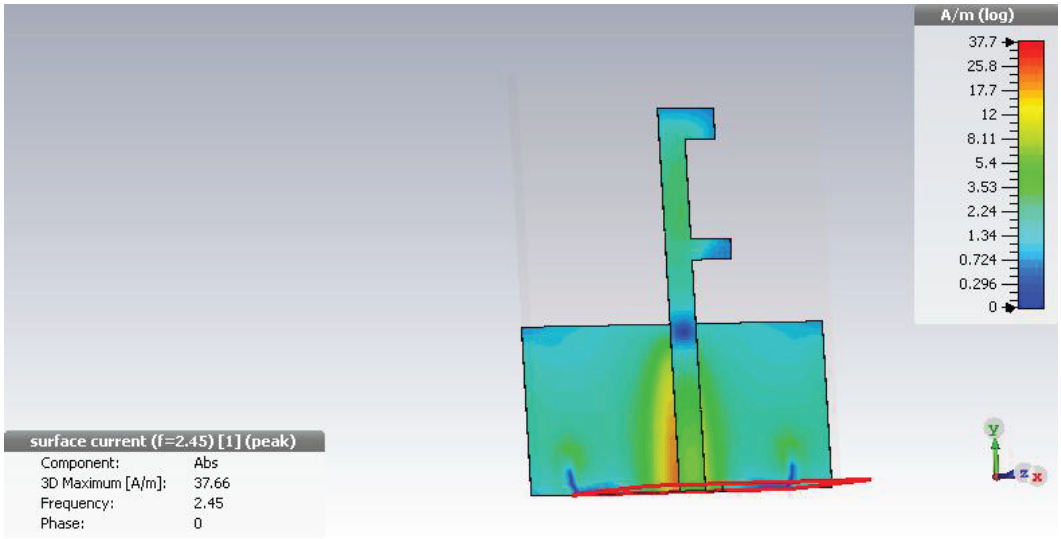

FIGURE 10. Surface current distribution for proposed antenna at 2.45 GHz.

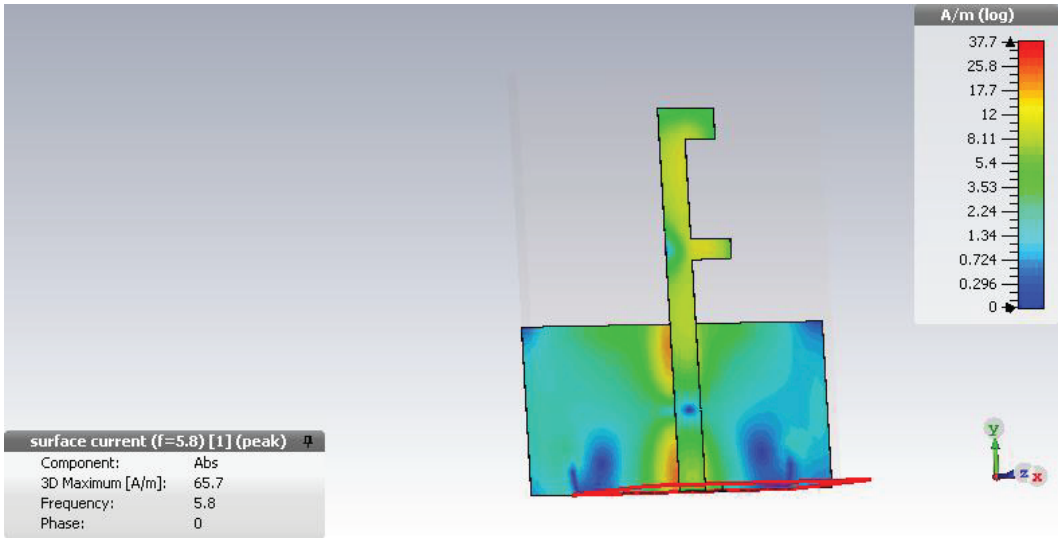

FIGURE 11. Surface current distribution for proposed antenna at 5.8 GHz.

6.5. ANN Results

A dataset consisting of 121 samples was utilized to train the ANN models. For the Feedforward Backpropagation Neural Network (FFBPN), the architecture was configured with 2 neurons in the input layer, 10 neurons in the hidden layer, and 2 neurons in the output layer. The training function used was `trainlm`, and the learning rate was set to 0.15. For training the General Regression Neural Network (GRNN), a spread constant of 1 was selected. Fig. 14 illustrates the performance plot of Mean Squared Error (MSE) versus the number of epochs. The best validation performance achieved was 3.9506×10^{-5} at epoch 21.

Tables 3 and 4 present the performance evaluation results of two different models using Mean Squared Error (MSE) and regression values across the training, validation, and testing phases for the General Regression Neural Network (GRNN) and Feedforward Backpropagation Neural Network (FFBPN), respectively.

Based on the evaluation results of both FFBPN and GRNN, it is observed that the FFBPN achieves lower MSE across all training, validation, and testing phases than GRNN. Since the primary objective of this work is the accurate prediction of resonant frequency values in antenna design, the accuracy of predicted values is crucial, making MSE the most significant indicator in this context.

Although the regression coefficient (R) is slightly higher in the GRNN model, this metric only measures the linear relationship between actual and predicted outputs and does not always reflect the magnitude of the absolute error. Therefore, considering the need for precise frequency prediction in antenna applications, where even small deviations are critical, the FFBPN model is more suitable due to its superior accuracy in absolute

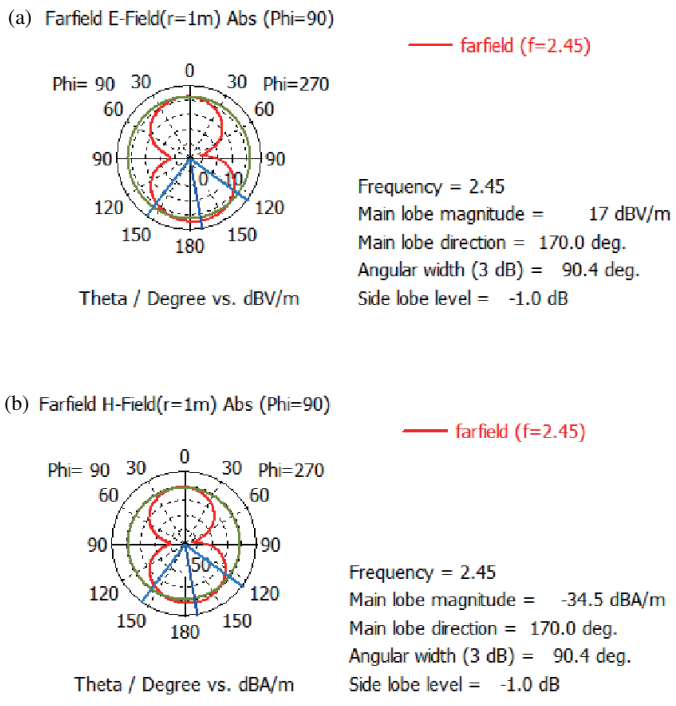

FIGURE 12. The E-plane and H-plane characteristics of the proposed antenna at 2.45 GHz.

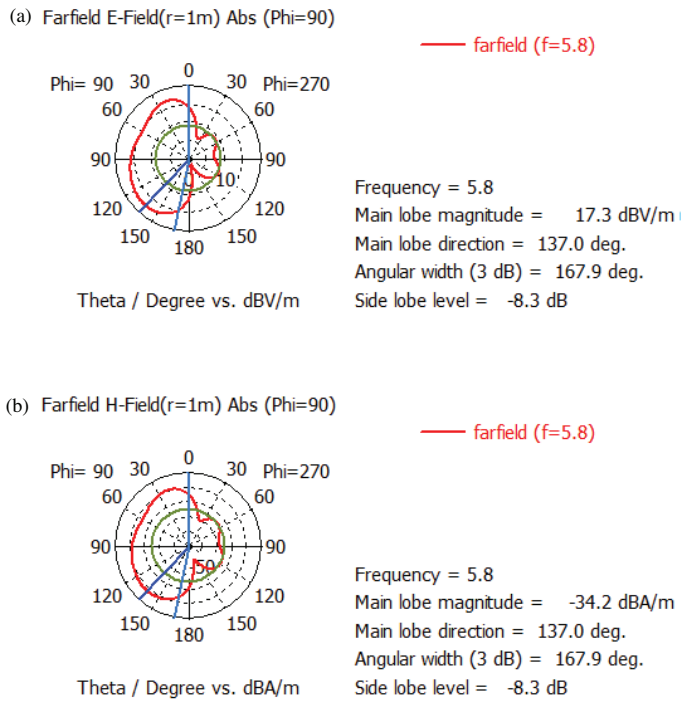

FIGURE 13. Characteristics of the proposed antenna at 2.45 GHz. (a) E-plane and (b) H-plane.

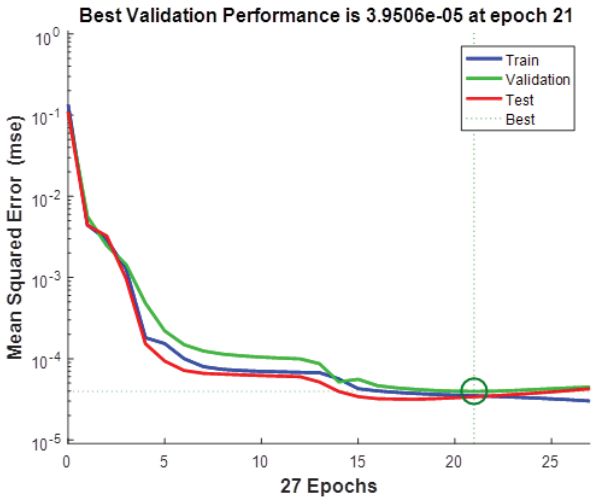

FIGURE 14. Mean Square Error (MSE) performance over epochs during training.

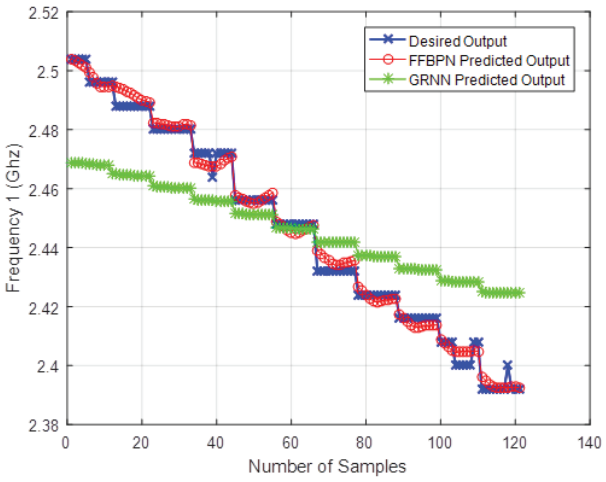

FIGURE 15. Comparison of ANN outputs with desired output for frequency 1

TABLE 3. Performance results in terms of MSE and regression for GRNN.

Phase	MSE	Regression
Train	0.0089717	0.99557
Validation	0.0094297	0.99901
Test	0.0085885	0.85399

TABLE 4. Performance results in terms of MSE and regression for FFBPN.

Phase	MSE	Regression
Train	2.5038×10^{-5}	0.99393
Validation	3.0653×10^{-5}	0.96992
Test	8.6203×10^{-5}	0.84270

value predictions, as confirmed by the plotted results and absolute error comparisons.

The performance of two distinct artificial neural networks (ANNs) was assessed using the same dataset. Tables 5 and 6 illustrate the comparison between FFBPN and GRNN outputs

TABLE 5. Comparison of desired and FFBPN outputs with errors.

L2	L3	Desired f1	Desired f2	FFBPN f1	FFBPN f2	Absolute Error1	Absolute Error2
3.5	4.8	2.448	5.728	2.4469	5.7299	0.0010575	0.0018825
4.1	4.2	2.416	5.912	2.4134	5.8983	0.0026017	0.013716
3.9	3.6	2.424	6.112	2.4228	6.1159	0.0011639	0.0038604
2.7	5.0	2.488	5.712	2.4894	5.7049	0.0013718	0.0070951
2.9	3.8	2.480	6.144	2.4814	6.1390	0.0013789	0.0050485
3.3	4.8	2.456	5.774	2.4578	5.7510	0.0018402	0.022974
3.5	4.0	2.448	6.016	2.4448	6.0221	0.0032136	0.0060647
2.5	4.0	2.496	6.112	2.4995	6.1165	0.0034875	0.0045105
3.3	4.4	2.456	5.896	2.4561	5.8908	0.0000626	0.0052446
3.1	3.2	2.472	6.344	2.4687	6.3356	0.0033413	0.0084424

TABLE 6. Comparison of desired and GRNN outputs with errors.

L2	L3	Desired f1	Desired f2	GRNN f1	GRNN f2	Absolute Error1	Absolute Error2
3.5	4.8	2.448	5.728	2.4464	5.8966	0.0016241	0.16857
4.1	4.2	2.416	5.912	2.4326	5.9594	0.0166010	0.047429
3.9	3.6	2.424	6.112	2.4372	6.0569	0.0131600	0.055131
2.7	5.0	2.488	5.712	2.4642	5.9001	0.0238080	0.18809
2.9	3.8	2.480	6.144	2.4605	6.0686	0.0195270	0.075398
3.8	4.8	2.456	5.774	2.4511	5.9042	0.0048849	0.13023
3.5	4.0	2.448	6.016	2.4465	6.0136	0.0015037	0.0023561
2.5	4.0	2.496	6.112	2.4683	6.0514	0.0276580	0.060625
3.3	4.4	2.456	5.896	2.4512	5.9607	0.0048282	0.064692
3.1	3.2	2.472	6.344	2.4563	6.1455	0.0157270	0.19847

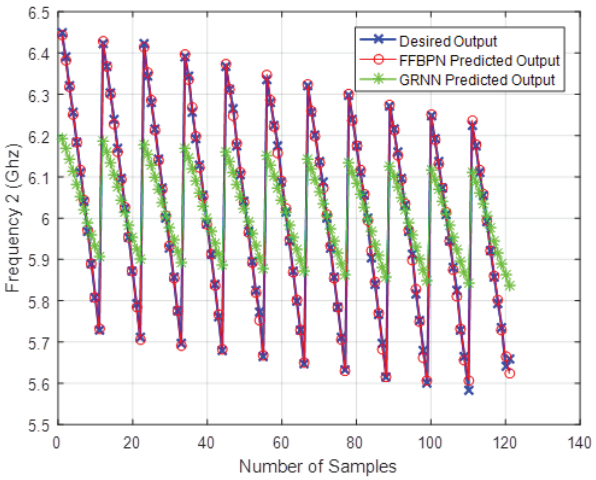

FIGURE 16. Comparison of ANN outputs with desired output for frequency 2.

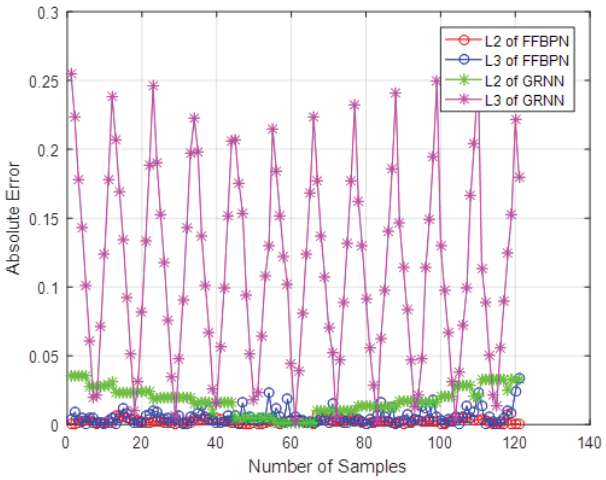

FIGURE 17. Comparison of errors of both ANNs versus number of samples.

TABLE 7. Average absolute errors for different networks.

Network	Avg Abs Error f1	Avg Abs Error f2
FFBPN	0.002292	0.0056708
GRNN	0.017468	0.1128900

against the desired outputs based on absolute error. Additionally, Table 7 provides a comparison of the average absolute errors for both ANNs with respect to f_{r1} and f_{r2}. The results indicate that FFBPN consistently exhibits lower average absolute errors than GRNN for both f_{r1} and f_{r2}. Consequently, FFBPN is favored over GRNN for this study. Figs. 15 and 16 present graphical comparisons of FFBPN and GRNN outputs against

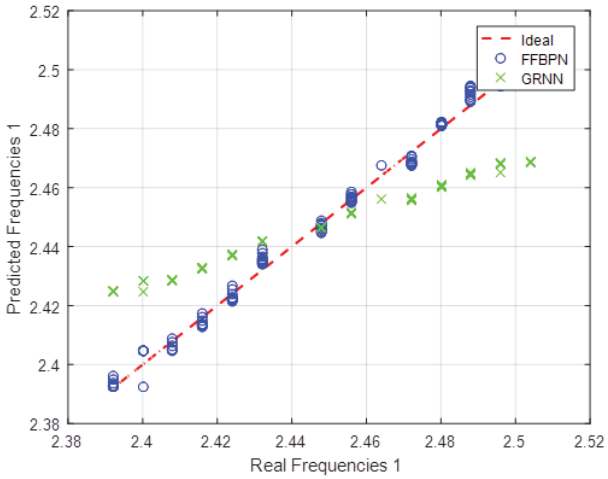

FIGURE 18. Predicted Frequencies 1 vs. Real Frequencies 1.

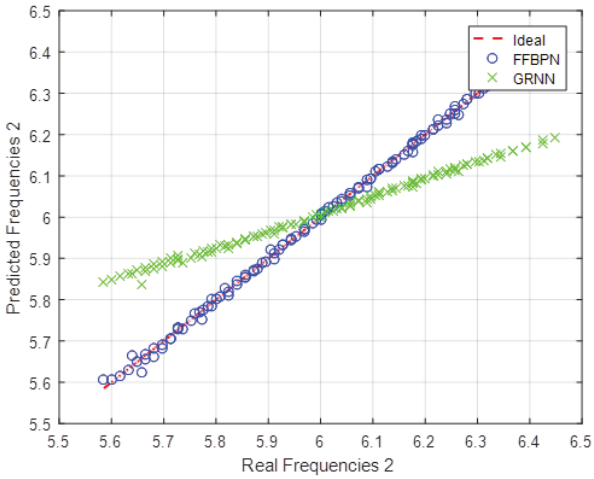

FIGURE 19. Predicted Frequencies 2 vs. Real Frequencies 2.

TABLE 8. Comparison between PSO by curve fitting and ANN highlighting the superiority of ANN.

PSO by Curve Fitting	ANN (Neural Network)
Searches for coefficients of a predefined function	Learns the relationship directly from the data
Limited to the chosen mathematical form	Can represent any linear or nonlinear relationship
Requires fewer data samples	Requires more data but utilizes it efficiently
Accuracy is medium and depends on the correctness of the function	Generally higher accuracy, especially when the relationship is unknown or complex

the desired outputs for f_{r1} and f_{r2}, respectively. Fig. 17 depicts a comparative analysis of the errors for both ANNs as a function of the number of samples.

6.6. PSO Results

The objective of Particle Swarm Optimization (PSO) is to optimize the parameter values L_2 and L_3 to achieve the desired resonance frequencies (f_{r1} and f_{r2}). The algorithm is initialized with a cohort of 40 particles and a maximum of 1000 iterations. The design parameters are established within suitable minimum and maximum limits, creating a two-dimensional search space for optimization. PSO subsequently identifies the optimal parameter values of the proposed antenna. The cost function determines that the optimal parameter values are $L_2 = 3.5\,\text{mm}$ and $L_3 = 4.6\,\text{mm}$.

6.7. Comparative Optimization Analysis

Table 8 summarizes the differences between PSO by curve fitting and ANN. While PSO depends on predefined mathematical functions and offers moderate accuracy with fewer data, ANN learns directly, from data, captures both linear and nonlinear relations, and generally provides higher accuracy for complex optimization problems.

Table 9 presents a comparison between the proposed antenna and currently existing antennas. A dual-band antenna is described in [58]; however, it exhibits a larger surface area than the proposed antenna. According to [33], the two-sleeve patch antenna is effective only for the ISM band and has a lower maximum realized gain than the proposed antenna. The antennas described in [34–37] operate within a single frequency band, and their dimensions are significantly larger than those of the proposed antenna. The antennas in [38–43] function at the 2.45 GHz ISM band, whereas the proposed antenna supports two ISM frequency bands. Hence, the proposed antenna offers several advantages over the antennas listed in Table 9, including smaller size, increased gain, improved efficiency, and enhanced compatibility with ISM frequency bands.

6.8. Antenna Prototype

The fabricated antenna is shown in Fig. 20. It is printed on an FR4 substrate and features an F-shaped radiating structure. This geometry is specifically designed to support dual-band operation at 2.45 GHz and 5.8 GHz.

Figure 21 illustrates the measurement setup used to evaluate the return loss (S_{11}) performance of the antenna. The device is connected to a Vector Network Analyzer (Agilent PNA-L) through a coaxial cable. To reduce undesired reflections and external interference, the antenna is placed on pyramidal RF absorbing foam during measurement.

The comparison between simulated and measured return loss results is presented in Fig. 22. Good agreement is observed between the two curves, with resonances appearing around 2.45 GHz and 5.8 GHz in both cases. Slight discrepancies in the return loss levels can be attributed to fabrication tolerances

TABLE 9. Comparison of proposed antenna with existing antennas.

Reference	Substrate Material	Volume (mm^3)	Frequency Band (GHz)	Design Description
[33]	FR4	1925.6	2.45 (ISM)	Two Sleeve Patch Geometry
[34]	FR4	62083.2	0.402–0.405 (MICS)	Fractal Cantor Design
[35]	Rogers 3210	10240	0.402–0.405 (MICS)	Spiral Radiator
[36]	Rogers 4350B	9534	2.4–2.5 (ISM)	L-Probe Circular Patch
[37]	FR4	9242	2.4–2.5 (ISM)	Rectangular Patch with Inset Feed
[38]	FR4	1624	2.45 (ISM)	U-shaped Meandered Patch
[39]	Copper clad	992	2.4–2.5 (ISM)	Rectangular Patch
[40]	FR4	768	2.45 (ISM)	Tree-shaped Hybrid Patch
[41]	Jean	800	2.45 (ISM)	Wearable PIFA
[42]	Rogers 3210	643	0.402–0.405 (MICS)	Π-shaped Patch with L-strips
[43]	FR4	588	2.4–2.48 (ISM)	Slotted Patch
[58]	FR4	2897.2	0.402–0.406 (MICS), 2.4–2.5 (ISM)	Spiral Patch
Proposed Antenna	FR4	2240	2.45 (ISM), 5.80 (ISM)	F-shaped Structure

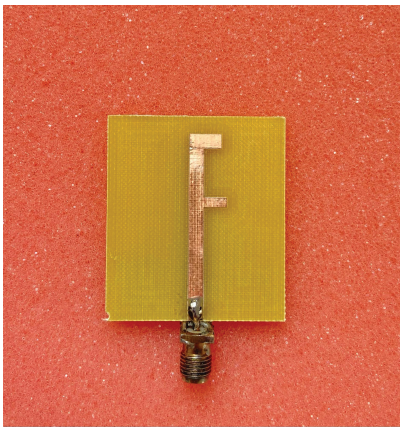

FIGURE 20. Top view of the fabricated F-shaped microstrip antenna.

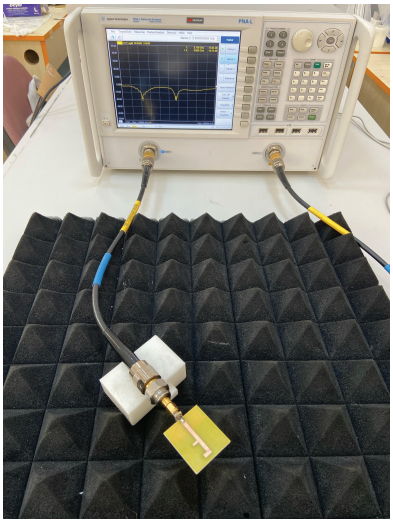

FIGURE 21. Measurement setup using a Vector Network Analyzer (VNA).

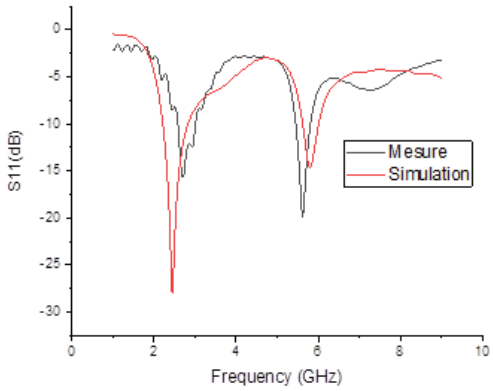

FIGURE 22. Comparison of simulated and measured S_{11} results.

and connector losses, which are common in practical implementations.

7. CONCLUSION

This paper presents an F-shaped compact dual-band monopole antenna optimized at 2.45/5.8 GHz ISM medical application using ANN and PSO approaches. The proposed antenna, which is printed on an FR4 substrate, features the frequencies of 2.448 GHz and 5.8 GHz with bandwidths of 610 MHz (2.21–-2.82 GHz) and 400 MHz (5.61-–6.01 GHz) with the gains of 2.262 dBi and 3.9 dBi. The PSO algorithm adjusted the patch parameters to $L_2 = 3.5$mm and $L_3 = 4.6$mm, whereas Feed-forward Backpropagation Neural Network (FFBPN) surpassed Generalized Regression Neural Network (GRNN) with a mean squared error of 3.9506×10^{-5}. Measurements from the fabricated prototype show excellent consistency with simulations, confirming the antenna's viability for wireless medical applications, such as wearable sensors and telemedicine devices. The constructed ANN-PSO approach is highly efficient and accurate, being a powerful technique for future optimization of antennas in biomedical engineering.

FUNDING

This publication has received funding from the European Union's Horizon Europe research and innovation program under grant agreement HE-MSCA-SE-6G-TERAFIT-101131501. This project received funding in part from the DGRSDT (Direction Générale de la Recherche Scientifique et du Développement Technologique), MESRS (Ministry of Higher Education and Scientific Research), Algeria.

ACKNOWLEDGEMENT

This research was additionally funded by the European Union's Horizon Europe research and innovation program through grant agreement HE-MSCA-SE-6G-TERAFIT-101131501, as well as by the General Directorate of Scientific Research and Technological Development (DGRSDT) — Ministry of Higher Education and Scientific Research.

REFERENCES

[1] Salhi, A., S. Maouni, I. Elfergani, C. Zebiri, J. Rodriguez, F. Gil-Castiñeira, Y. A. Mousa, and A. Varshney, "Design of a compact UWB SISO antenna for enhanced wireless communication systems," in *2024 International Conference on Advances in Electrical and Communication Technologies (ICAECOT)*, 1–4, Setif, Algeria, 2024.

[2] Wang, Z. D., Y. Z. Yin, X. Yang, and J. J. Wu, "Design of a wideband horizontally polarized omnidirectional antenna with mutual coupling method," *IEEE Transactions on Antennas and Propagation*, Vol. 63, No. 7, 3311–3316, 2015.

[3] Alaoui, N., B. A. Amel, and Z. Aya, "Tri-band frequency reconfigurable antenna for wireless applications," *Instrumentation, Mesures, Métrologies*, Vol. 23, No. 2, 175–182, 2024.

[4] Melvin, W. L., J. Scheer, *et al.*, *Principles of Modern Radar*, Scitech Pub., 2013.

[5] Eaves, J. and E. Reedy, *Principles of Modern Radar*, Springer Science & Business Media, 2012.

[6] Kiourti, A. and K. S. Nikita, "A review of implantable patch antennas for biomedical telemetry: Challenges and solutions [wireless corner]," *IEEE Antennas and Propagation Magazine*, Vol. 54, No. 3, 210–228, 2012.

[7] Hall, P. S. and Y. Hao, *Antennas and Propagation for Body-Centric Wireless Communications*, Artech House, 2012.

[8] Hirata, A., Y. Diao, T. Onishi, K. Sasaki, S. Ahn, D. Colombi, V. D. Santis, I. Laakso, L. Giaccone, W. Joseph, *et al.*, "Assessment of human exposure to electromagnetic fields: Review and future directions," *IEEE Transactions on Electromagnetic Compatibility*, Vol. 63, No. 5, 1619–1630, 2021.

[9] Zebiri, C., S. Mekki, D. Sayad, I. Elfergani, M. L. Bouknia, R. Zegadi, A. Varshney, and J. Rodriguez, "Low SAR-UWB rectangular microstrip magnetic monopole antenna for S-band and biomedical applications," *Applied Computational Electromagnetics Society Journal (ACES)*, Vol. 40, No. 3, 212–225, 2025.

[10] Singh, S., A. Varshney, V. Sharma, I. Elfergani, C. Zebiri, and J. Rodriguez, "A compact off-set edge fed odd-symmetric hybrid fractal slotted antenna for UWB and space applications," *Progress In Electromagnetics Research B*, Vol. 102, 37–60, 2023.

[11] Mehenni, N.-E., S. Khacha, Y. Teghilt, R. Zegadi, and C. Zebiri, "Miniaturized ultra-wideband rectangular patch antenna for breast tumor detection," in *2024 International Conference on Advances in Electrical and Communication Technologies (ICAECOT)*, 1–5, Setif, Algeria, 2024.

[12] Elfergani, I., A. Iqbal, C. Zebiri, A. Basir, J. Rodriguez, M. Sajedin, A. d. O. Pereira, W. Mshwat, R. Abd-Alhameed, and S. Ullah, "Low-profile and closely spaced four-element MIMO antenna for wireless body area networks," *Electronics*, Vol. 9, No. 2, 258, 2020.

[13] Islam, M. S., S. M. K. Azam, A. K. M. Z. Hossain, M. I. Ibrahimy, and S. M. A. Motakabber, "A low-profile flexible planar monopole antenna for biomedical applications," *Engineering Science and Technology, an International Journal*, Vol. 35, 101112, 2022.

[14] Al-Sehemi, A., A. Al-Ghamdi, N. Dishovsky, N. Atanasov, and G. Atanasova, "A flexible miniature antenna for body-worn devices: Design and transmission performance," *Micromachines*, Vol. 14, No. 3, 514, 2023.

[15] Kiourti, A. and K. S. Nikita, "A review of in-body biotelemetry devices: Implantables, ingestibles, and injectables," *IEEE Transactions on Biomedical Engineering*, Vol. 64, No. 7, 1422–1430, 2017.

[16] Kiourti, A. and K. S. Nikita, "Miniature scalp-implantable antennas for telemetry in the MICS and ISM bands: Design, safety considerations and link budget analysis," *IEEE Transactions on Antennas and Propagation*, Vol. 60, No. 8, 3568–3575, 2012.

[17] Azzouz, A., B. Bengherbia, P. Wira, N. Alaoui, A. Souahlia, M. Maazouz, and H. Hentabeli, "An efficient ECG signals denoising technique based on the combination of particle swarm optimisation and wavelet transform," *Heliyon*, Vol. 10, No. 5, e26171, 2024.

[18] Abdallah, A., B. Billel, A. Nail, and S. Abdelkerim, "ECG signal denoising based on wavelet transform and genetic algorithm," in *2023 International Conference on Advances in Electronics, Control and Communication Systems (ICAECCS)*, 1–6, Blida, Algeria, 2023.

[19] Azzouz, A., B. Bengherbia, P. Wira, N. Alaoui, and A. Souahlia, "The effectiveness of optimal discrete wavelet transform parameters obtained using the genetic algorithm for ECG signal denoising," *Revue D'intelligence Artificielle*, Vol. 37, No. 6, 1387–1396, 2023.

[20] Weinstein, R. S., A. M. Lopez, B. A. Joseph, K. A. Erps, M. Holcomb, G. P. Barker, and E. A. Krupinski, "Telemedicine, telehealth, and mobile health applications that work: Opportunities and barriers," *The American Journal of Medicine*, Vol. 127, No. 3, 183–187, 2014.

[21] Baig, M. M., H. GholamHosseini, A. A. Moqeem, F. Mirza, and M. Lindén, "A systematic review of wearable patient monitoring systems-current challenges and opportunities for clinical adoption," *Journal of Medical Systems*, Vol. 41, No. 7, 115, 2017.

[22] Ali, U., S. Ullah, B. Kamal, L. Matekovits, and A. Altaf, "Design, analysis and applications of wearable antennas: A review," *IEEE Access*, Vol. 11, 14 458–14 486, 2023.

[23] Mohamadzade, B., R. M. Hashmi, R. B. V. B. Simorangkir, R. Gharaei, S. U. Rehman, and Q. H. Abbasi, "Recent advances in fabrication methods for flexible antennas in wearable devices: State of the art," *Sensors*, Vol. 19, No. 10, 2312, 2019.

[24] El Gharbi, M., R. Fernández-García, S. Ahyoud, and I. Gil, "A review of flexible wearable antenna sensors: Design, fabrication methods, and applications," *Materials*, Vol. 13, No. 17, 3781, 2020.

[25] Balanis, C. A., *Antenna Theory: Analysis and Design*, John Wiley & Sons, 2016.

[26] Chahat, N., M. Zhadobov, R. Sauleau, and K. Ito, "A compact UWB antenna for on-body applications," *IEEE Transactions on Antennas and Propagation*, Vol. 59, No. 4, 1123–1131, 2011.

[27] Slimani, A., C. Zebiri, S. Khacha, F. Kerrour, D. Sayad, K. Karacuha, I. Elfergani, and J. Rodriguez, "A compact UWB textile antenna designed for WLAN and C-band applications," in *2025 19th European Conference on Antennas and Propagation (EuCAP)*, 1–5, Stockholm, Sweden, 2025.

[28] Finkenzeller, K. and D. Müller, *RFID Handbook: Fundamentals and Applications in Contactless Smart Cards, Radio Frequency Identification and Near-Field Communication*, 3rd edition, 2010.

[29] Lizzi, L. and A. Massa, "Dual-band printed fractal monopole antenna for LTE applications," *IEEE Antennas and Wireless Propagation Letters*, Vol. 10, 760–763, 2011.

[30] Hu, X.-Y., W.-L. Yin, F. Du, C. Zhang, P. Xiao, and G. Li, "Biomedical applications and challenges of in-body implantable antenna for implantable medical devices: A review," *AEU — International Journal of Electronics and Communications*, Vol. 174, 155053, 2024.

[31] Kumar, S. A. and T. Shanmuganantham, "Design of implantable cpw fed monopole h-slot antenna for 2.45 GHz ISM band applications," *AEU — International Journal of Electronics and Communications*, Vol. 68, No. 7, 661–666, 2014.

[32] Al-Hasan, M., P. R. Sura, A. Iqbal, J. J. Tiang, I. B. Mabrouk, and M. Nedil, "Low-profile dual-band implantable antenna for compact implantable biomedical devices," *AEU — International Journal of Electronics and Communications*, Vol. 138, 153896, 2021.

[33] Sukhija, S. and R. K. Sarin, "Design and performance of two-sleeve low profile antenna for bio-medical applications," *Journal of Electrical Systems and Information Technology*, Vol. 4, No. 1, 49–61, 2017.

[34] Srivatsun, G., S. S. Rani, and G. S. Krishnan, "A self-similar fractal Cantor antenna for MICS band wireless applications," *Wireless Engineering and Technology*, Vol. 2, No. 2, 2011.

[35] Kim, J. and Y. Rahmat-Samii, "Implanted antennas inside a human body: Simulations, designs, and characterizations," *IEEE Transactions on Microwave Theory and Techniques*, Vol. 52, No. 8, 1934–1943, 2004.

[36] Lin, W. and H. Wong, "Polarization reconfigurable circular patch antenna with multiple L-probes for biomedical application," in *2016 IEEE International Symposium on Antennas and Propagation (APSURSI)*, 1669–1670, Fajardo, PR, USA, 2016.

[37] Çalışkan, R., S. S. Gültekin, D. Uzer, and O. Dündar, "A microstrip patch antenna design for breast cancer detection," *Procedia — Social and Behavioral Sciences*, Vol. 195, 2905–2911, 2015.

[38] Sukhija, S. and R. K. Sarin, "A U-shaped meandered slot antenna for biomedical applications," *Progress In Electromagnetics Research M*, Vol. 62, 65–77, 2017.

[39] Shrestha, S., M. Agarwal, P. Ghane, and K. Varahramyan, "Flexible microstrip antenna for skin contact application," *International Journal of Antennas and Propagation*, Vol. 2012, No. 1, 745426, 2012.

[40] Kaur, M. and J. S. Sivia, "Tree-shaped hybrid fractal antenna for biomedical applications using ANN and PSO," *Wireless Personal Communications*, 2021.

[41] Gil, I. and R. Fernández-García, "Wearable PIFA antenna implemented on jean substrate for wireless body area network," *Journal of Electromagnetic Waves and Applications*, Vol. 31, No. 11-12, 1194–1204, 2017.

[42] Lee, C.-M., T.-C. Yo, F.-J. Huang, and C.-H. Luo, "Dual-resonant π-shape with double L-strips PIFA for implantable biotelemetry," *Electronics Letters*, Vol. 44, No. 14, 837–839, 2008.

[43] Kumar, S. A. and T. Shanmuganantham, "Implantable CPW-fed rectangular patch antenna for ISM band biomedical applications," *International Journal of Microwave and Wireless Technologies*, Vol. 6, No. 1, 101–107, 2014.

[44] Maouni, S., A. Salhi, I. Elfergani, C. Zebiri, J. Rodriguez, F. Gil-Castiñeira, Y. A. Mousa, and A. Varshney, "Miniaturized biomedical wearable patch antenna design with low SAR content," in *2024 International Conference on Advances in Electrical and Communication Technologies (ICAECOT)*, 1–6, Setif, Algeria, 2024.

[45] Wong, H., K.-M. Luk, C. H. Chan, Q. Xue, K. K. So, and H. W. Lai, "Small antennas in wireless communications," *Proceedings of the IEEE*, Vol. 100, No. 7, 2109–2121, 2012.

[46] Wong, K.-L. and C.-H. Chang, "WLAN chip antenna mountable above the system ground plane of a mobile device," *IEEE Transactions on Antennas and Propagation*, Vol. 53, No. 11, 3496–3499, 2005.

[47] Yang, H. Y. D., "Miniaturized printed wire antenna for wireless communications," *IEEE Antennas and Wireless Propagation Letters*, Vol. 4, 358–361, 2005.

[48] Ali, M. and G. J. Hayes, "Small printed integrated inverted-F antenna for Bluetooth application," *Microwave and Optical Technology Letters*, Vol. 33, No. 5, 347–349, 2002.

[49] Soras, C., M. Karaboikis, G. Tsachtsiris, and V. Makios, "Analysis and design of an inverted-F antenna printed on a PCMCIA card for the 2.4 GHz ISM band," *IEEE Antennas and Propagation Magazine*, Vol. 44, No. 1, 37–44, 2002.

[50] Jung, J., H. Lee, and Y. Lim, "Compact monopole antenna for dual ISM-bands (2.4 and 5.8 GHz) operation," *Microwave and Optical Technology Letters*, Vol. 51, No. 9, 2227–2229, 2009.

[51] Yu, X., G. Li, and Z. Wang, "Design of compact 2.45 GHz microstrip antenna," in *2005 IEEE International Symposium on Microwave, Antenna, Propagation and EMC Technologies for Wireless Communications*, Vol. 1, 153–156, Beijing, China, 2005.

[52] Praveen Kumar, A. V., V. Hamsakutty, J. Yohannan, and K. T. Mathew, "Microstripline-fed half-cylindrical dielectric resonator antenna for 2.4-GHz WLAN application," *Microwave and Optical Technology Letters*, Vol. 48, No. 4, 724–726, 2006.

[53] Sabban, A., "New wideband printed antennas for medical applications," *IEEE Transactions on Antennas and Propagation*, Vol. 61, No. 1, 84–91, 2012.

[54] Bouknia, M. L., I. Elfergani, C. Bensid, J. Rodriguez, R. Zegadi, C. Zebiri, and D. Sayad, "Design of a novel mmwave defected ground structure based elliptical microstrip patch antenna for body-centric communications," in *2024 International Conference on Advances in Electrical and Communication Technologies (ICAECOT)*, 1–5, Setif, Algeria, 2024.

[55] Mekki, S., A. Varshney, D. Sayad, I. Elfergani, H. Bendjedi, M. L. Bouknia, R. Zegadi, J. Rodriguez, M. Palandoken, K. Karaçuha, and C. Zebiri, "Design and investigation of orthogonal hybrid dual-mode single-CDR-based MIMO antenna with high self-isolation at 5.8 GHz," *IEEE Access*, Vol. 12, 187 234–187 254, 2024.

[56] Dhaliwal, B. S. and S. S. Pattnaik, "Performance comparison of bio-inspired optimization algorithms for sierpinski gasket fractal antenna design," *Neural Computing and Applications*, Vol. 27, No. 3, 585–592, 2016.

[57] Dhaliwal, B. S. and S. S. Pattnaik, "Development of PSO-ANN ensemble hybrid algorithm and its application in compact crown circular fractal patch antenna design," *Wireless Personal Communications*, Vol. 96, No. 1, 135–152, 2017.

[58] Salim, M. and A. Pourziad, "A novel reconfigurable spiral-shaped monopole antenna for biomedical applications," *Progress In Electromagnetics Research Letters*, Vol. 57, 79–84, 2015.

[59] Anguera, J., A. Andújar, J. Jayasinghe, V. V. S. S. S. Chakravarthy, P. S. R. Chowdary, J. L. Pijoan, T. Ali, and C. Cattani, "Fractal antennas: An historical perspective," *Fractal and Fractional*, Vol. 4, No. 1, 3, 2020.

[60] Melouka, R. I. B., Y. Tighilt, C. Zebiri, K. Karaçuha, A. F. Hamida, A. Mashat, and N. Alaoui, "Biomedical antenna design optimization using multi-objective inverse neural networks," *Progress In Electromagnetics Research C*, Vol. 154, 47–59, 2025.

[61] Thakare, V. V. and P. Singhal, "Microstrip antenna design using artificial neural networks," *Co-sponsored by the Center for Advanced Manufacturing and Packaging of Microwave, Optical, and Digital Electronics (Campmode) at the University of Colorado at Boulder*, Vol. 20, No. 1, 76–86, 2010.

[62] Mamta, K., R. K. Singh, N. K. Sinha, and R. K. Keshri, "Design and development of microstrip patch antenna for millimeter-wave application," in *Proceeding of the Second International Conference on Microelectronics, Computing & Communication Systems (MCCS 2017)*, 79–85, 2018.

[63] Feiz, N., F. Mohajeri, and D. Zarifi, "Design, simulation and fabrication of an optimized microstrip antenna with metamaterial superstrate using particle swarm optimization," *Progress In Electromagnetics Research M*, Vol. 36, 101–108, 2014.